



Design and control of a spherical air-bearing system for multi-d.o.f. ball-joint-like actuators

Kok-Meng Lee *, Dan E. Ezenekwe, Tian He

*Georgia Institute of Technology, The George W. Woodruff School of Mechanical Engineering,
Atlanta, GA 30332-0405, USA*

Received 28 August 2000; accepted 26 March 2001

Abstract

This paper presents an analytical investigation of the design method and modeling of an air-bearing system for ball-joint-like actuators. It addresses the method of regulating the three-d.o.f. translations of the rotor introduced by the air-bearing system, thereby improving the dynamic performance of the orientation motion manipulation. The kinematics, which relates the rotor displacement and the air gaps that are essential for design optimization, dynamic simulation and motion control, are derived in closed-form. With a detailed modeling of the pressure–flow relationship as a function of the rotor position, the forces and dynamics of the system are formulated, and design methods for regulating the rotor displacement have been explored analytically. Simulation results suggest that the fluid forces could be generated to passively stabilize the otherwise open-loop, unstable, electromagnetic system. It is expected that this research will be a basis for designing and evaluating an improved VR spherical motor with enhanced torque capability by eliminating mechanical friction.

© 2002 Elsevier Science Ltd. All rights reserved.

1. Introduction

Many applications in industry require the use of fluid bearings to overcome friction, to provide more precise location and alignment of components, and to enable smooth movement of large components from one point to another point. In other applications, precise alignment of parts is critical to the quality and specifications of the product. As advances in technology continue to demand more accurate and

* Corresponding author. Tel.: +1-404-894-7402; fax: +1-404-894-9342.
E-mail address: kokmeng.lee@me.gatech.edu (K.-M. Lee).

precise devices, there are opportunities to utilize the uniquely attractive features of air-bearing systems to meet these challenges.

Three basic techniques are used in non-contact bearing designs. They are fluid bearings, magnetic levitation, and the Meissner effect. A comparison of the attributes of these levitation techniques is provided in Table 1 [1]. A non-contact air bearing is considered here, since it has the potential to enhance the motor's performance for more advanced applications, it has a cooling effect on interacting components and it does not interfere with the actuator electromagnetic system. In fluid bearings, a film of fluid is forced between interacting surfaces to separate them. An external pump usually generates the pressure. Depending on the source of pressurization, fluid bearings are categorized into hydrodynamic and hydrostatic bearings. Hydrodynamic bearings are self-acting since the pressure separating the surfaces is a consequence of high-frequency, relative oscillatory movement of the surfaces. This technique is commonly used in miniaturized, low load support applications, for example bearings for hard-disk drives [2]. In hydrostatic fluid bearings, external fluids, typically liquid oils, are supplied to maintain a high-pressurized fluid film between surfaces. The equivalent of hydrostatic and hydrodynamic bearings when air is the fluid medium are aerostatic and aerodynamic bearings, respectively. The primary difference is that air is compressible while liquids are generally considered incompressible.

Many authors have studied the dynamic behavior of fluid films in fluid-bearing systems [1,3]. Bearings based on viscous oil form the thrust of successes in heavy machinery design, where the oil films are used as friction-reducing, parts-separating lubricants especially in journal and ball bearings. Among the works in this area is the squeeze film technique motivated by the rapid advancement of micro-devices. Fearing et al. [4] studied miniaturized systems with small dimensions and narrow gaps associated with microstructures based on aerodynamic squeeze film technique and showed that the degree of pressurization is proportional to the frequency and amplitude of the externally applied oscillation. The researchers also extended the

Table 1
Comparison of levitation techniques

| Attributes | Fluid bearing | | Magnetic bearing | Meissner effect |
|---------------------------|---------------|---------|------------------|-----------------|
| | Gas | Oil | | |
| Simplicity | Fair | Fair | Good | – |
| Cleanliness | Good | Poor | Good | Good |
| Material availability | Good | Good | Fair | Poor |
| Cost | Average | Average | High | High |
| Load bearing | Poor | Good | – | – |
| Wear resistance | Good | Fair | Good | Good |
| Reliability | – | Fair | Fair | – |
| Operating temperature | Low | High | Low | Sub-zero |
| Heat dissipation | High | Fair | low | – |
| Standard parts available? | Poor | Good | Fair | – |
| Machining accuracy | High | High | – | – |

works of others by using capacitive measurements to study the stability of squeeze film bearings; they concluded that air spring force is proportional to the inverse fifth power of the plate separation while the damping force is proportional to the cube of the float height. Pina da Silva and his co-workers [5,6] presented a finite element method used for improving squeeze film analysis. Crank and Nicolson [7] had earlier contributed a method to vary design parameters in squeeze film bearings resulting in the effects of bearing parameters on the system performance being studied for improvements through optimization. Blech [8] developed and solved the linearized model for compressible gas lubrications while Sherman [9] extended the work to non-linear models. These works have contributed to sub-millimeter robotic systems like micro-robots.

Recently, Zorge [10] presented a method for measurement of miniature hemispherical air-bearing parameters such as load capacity, stiffness, etc., using electrical gap capacitance. The research showed that this method is inexpensive, has high measuring resolution and accuracy, and is able to capture dynamic behavior. The disadvantage of this method is that calibration is required for each bearing shape. In addition, the material of the bearing must not be metal, which is not always the practical case. On aerostatics, many researchers [11–13] have investigated bearing designs and characteristics. Ono [14] proposed an air bearing with multiple source feeds or narrow grooves to fight pneumatic instability; this design attained a measure of success. Other authors [12,15,16] have contributed to improving stability of fixed orifice or inherent restrictor bearings. Because self-excited vibrations may occur in frequently used fixed-orifice, aerostatic bearings, simultaneous improvements in the dynamic stiffness and stability were difficult to obtain. Sato et al. [17] examined theoretically and experimentally the dynamic characteristics with an actively controlled restrictor. Their results showed improvements in dynamic stiffness and stability. Though the experiment had some success, practical applications were not thought to be feasible. A drawback of aerostatic bearings is that relatively large areas are required to achieve high load-bearing capacity.

Other researchers have worked on controls techniques for bearing devices. Hammer et al. [18] designed a novel three-degrees of freedom (d.o.f.) fine positioner (FP), which provided high performance, precision and speed ($12g$'s acceleration, $0.2\ \mu\text{m}$ resolution) for robotic application. Control issues, aimed at achieving stable response, good disturbance rejection and closed-loop control, were discussed. Interests in developing integrated motor-bearing system have motivated a number of researchers [19–21] to develop control methods for magnetic bearing systems to compensate rotor misalignment. These works, however, have concentrated on single axis bearing devices.

In this paper, we explore the use of a non-contact, spherical air-bearing system for multi-d.o.f. spherical actuators developed by Lee and his co-workers [22–24], which operates on the principles of variable reluctance (VR). The motor combines the roll, pitch and yaw motion in one joint making it attractive for many applications. Besides the capability of three-d.o.f. motions in one joint, the motor has a large range of motion, isotropic properties and no singularities within the workspace. These flexible design features make the VR spherical motor suitable for a wide range of

applications such as water-jet cutting, laser cutting, painting, welding, material handling, coordinate measurement etc., where smooth uniform manipulation of the end-effector is required. Over the years, research has been directed toward the optimization of the motor torque. Recent efforts to reduce the discrepancies between the actual and predicted torque outputs have suggested that friction, accountable by the transfer bearings of the motor, is significant. While the “reaction-free” magnetic levitation control strategy proposed by Zhou and Lee [25] has the effect of relaxing frictional forces, the trade-off is the need for sophisticated feedback control design due to the inherent instability of the electromagnetic system. As advances in technology continue to demand more accurate and high precision spherical devices, we explore the use of thin-film air bearings along with the unique attractive features of the VR spherical motor to meet these challenges. Specifically, we discuss a practical means to effectively overcome static and dynamic friction in spherical actuators, aimed at improving the output torque and broadening the tasks they can undertake. We explore air bearings over fluid bearings, magnetic levitation, and the Meissner effect because air bearings are clean, have a cooling effect on interacting components and do not interfere with the actuator electromagnetic system.

The rest of this paper is organized as follows: Section 2 discusses the bearing design configuration for a ball-joint-like spherical device. This is followed by the characterization of airflow through the bearing in Section 3, which generates the forces on the rotor. Then, the system dynamics are presented in Section 4, followed by design methodology and simulations in Section 5. Finally, our conclusions are presented.

2. Bearing for ball-joint-like devices

Consider an arbitrary displacement of the two spherical surfaces as shown in Fig. 1, where \vec{r}_o is the rotor displacement with respect to the center of the stator.

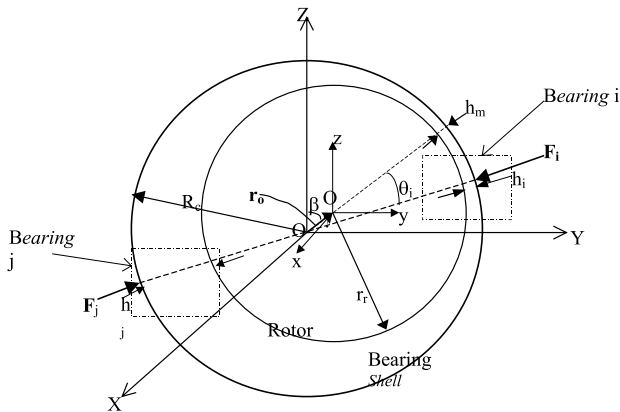


Fig. 1. Conceptual schematics illustrating spherical bearing.

In Fig. 1, the reference frame XYZ is defined at the center of the stator, O , with the Z -axis pointing toward the opening on the stator, and xyz is fixed at the center of the rotor, O' , with its z -axis along the rotor output shaft. At equilibrium, the coordinate frames XYZ and xyz have a common origin at their centers. Thus, any position on the rotor can be expressed with respect to the XYZ coordinate system using a 4×4 homogeneous transformation matrix, $[T]$:

$$[P]_{XYZ} = [T][P]_{xyz}, \quad (1)$$

where $[P]_{XYZ}$ and $[P]_{xyz}$ are the position of a point on the rotor measured with respect to XYZ and xyz , respectively.

2.1. Bearing configurations

The design concept uses pressurized air to regulate the rotor such that the rotor displacement \bar{r}_o is null regardless of any “disturbances” caused by the electromagnetic actuation or an external force. Multiple independent spherical bearings are strategically designed to support the rotor. In general, the larger the number of bearings, the larger the load the system is capable of supporting. The challenge, however, is to design a compact yet efficient air-bearing system to fit into the limited surface area of the rotor. In addition, the bearings should be designed so that they do not interfere with the electromagnetic poles of the spherical motor, which are located following the pattern of a regular polyhedron.

An attractive design forces pressurized air passes through the center of the stator poles on which the coils are wound, enabling the units to serve as bearings. The advantages of joint magnetic-pole/bearing units are twofold: (1) The air jet will provide a cooling effect to the coil windings. (2) It will optimize the stator surface by maximizing the size of a bearing, thereby enhancing load-bearing capacity. In the following discussion, we shall consider the case where six or more bearing points are evenly spaced on the spherical bearing such that bearing forces can always be grouped in pairs. As illustrated in Fig. 1, the pair of bearing forces \bar{F}_i and \bar{F}_j exert equal but opposite forces through the center of the stator.

2.2. Forward kinematics

The gap between the stator and rotor along a pair of forces, \bar{F}_i and \bar{F}_j , can be determined with the aid of Fig. 2. The net force, $\bar{F}_{ij} = \bar{F}_i + \bar{F}_j$, can be described by

$$\bar{F}_{ij} = F_{ij}\bar{e}_{ij}, \quad (2)$$

where F_{ij} and \bar{e}_{ij} are the magnitude and the unit vector (known) of the resultant force. As shown graphically in Fig. 2(b), the minimum air gap between the rotor and the stator is in the direction of \bar{r}_o . Thus, the included angle between \bar{F}_{ij} and \bar{r}_o is

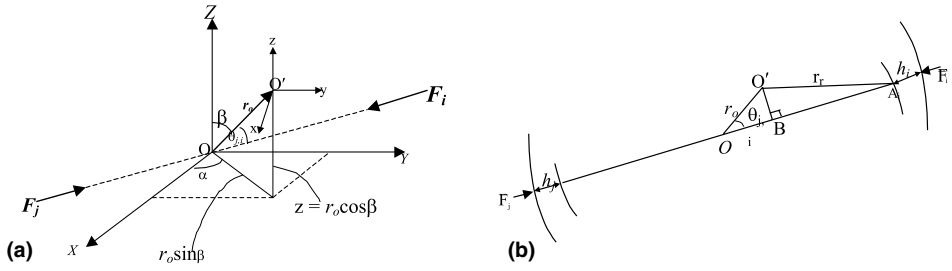


Fig. 2. Schematics for gap determination. (a) Rotor displacement. (b) Bearing force line of action.

$$\theta_{ji} = \cos^{-1} \left(\bar{e}_{ij} \cdot \bar{e}_{r_o} \right) = \cos^{-1} \left(\frac{\bar{F}_{ij} \cdot \bar{r}_o}{F_{ij} r_o} \right), \tag{3}$$

where r_o is the magnitude and \bar{e}_{r_o} is the unit vector of \bar{r}_o . For a given rotor displacement, the air gaps, h_i , and h_j are given by Eqs. (4a) and (4b):

$$h_i = r_s - \left\{ \sqrt{r_r^2 - r_o^2 \sin^2 \theta_{ji}} + r_o \cos \theta_{ji} \right\} \tag{4a}$$

and

$$h_j = r_s - \left\{ \sqrt{r_r^2 - r_o^2 \sin^2 \theta_{ji}} - r_o \cos \theta_{ji} \right\}, \tag{4b}$$

where r_s and r_r are the radii of the stator and rotor at the interface, respectively.

2.3. Inverse kinematics

Since direct sensing of the rotor displacement \bar{r}_o is difficult, the inverse kinematics provide a practical means of computing the rotor position from the air gap measurements. With three independent pairs of gap measurements, the three orthogonal components of the rotor displacement can be determined as follows.

Subtracting Eq. (4a) from Eq. (4b), we have

$$r_o \cos \theta_{ji} = \bar{r}_o \cdot \bar{e}_{ij} = \frac{h_j - h_i}{2}. \tag{5a}$$

Two other similar equations can be obtained from two other pairs of air gaps.

$$\bar{r}_o \cdot \bar{e}_{j-1,i-1} = \frac{h_{j-1} - h_{i-1}}{2}, \tag{5b}$$

$$\bar{r}_o \cdot \bar{e}_{j+1,i+1} = \frac{h_{j+1} - h_{i+1}}{2}. \tag{5c}$$

Eqs. (5a)–(5c) can be written in matrix form:

$$\begin{bmatrix} \bar{e}_{j-1,i-1} & \bar{e}_{j,i} & \bar{e}_{j+1,i+1} \end{bmatrix} \begin{bmatrix} r_x \\ r_y \\ r_z \end{bmatrix} = \frac{1}{2} \begin{bmatrix} h_{j-1} - h_{i-1} \\ h_j - h_i \\ h_{j+1} - h_{i+1} \end{bmatrix}, \tag{6}$$

where r_x , r_y and r_z are the components of \bar{r}_o in the direction of X , Y and Z , respectively.

3. Air-bearing force model

Fig. 3 shows a schematic of a simple, pocketed, orifice-compensated bearing. Air enters from a pressure source, passes through an orifice of diameter d_o , then expands isentropically into the pocket of diameter R_p and recess d_p , and finally exhausts to the atmosphere through the annulus, which consists of two parallel surfaces of spacing h .

3.1. Flow characteristics

The following assumptions are made in deriving the dynamic model: (1) The pressure in the pocket is uniform; (2) The air is isothermal; (3) Changes in air density are attributed mainly to variations in pressure, and the ideal gas law, $p = \rho RT$, where p , R and T are the pressure, gas constant and temperature of the air, respectively, is assumed to hold throughout. Thus, the force acting on the rotor is given by integrating the pressure over the bearing surface as follows:

$$f = 2\pi \left[\int_0^{R_p} p_p r dr + \int_{R_p}^{R_b} p r dr \right], \tag{7}$$

where p_p and p are the pressures in the pocket and the annulus, respectively. The mass m contained in the bearing is a function of the rotor displacement along the direction of the actuating force as well as the air density and the state of the air.

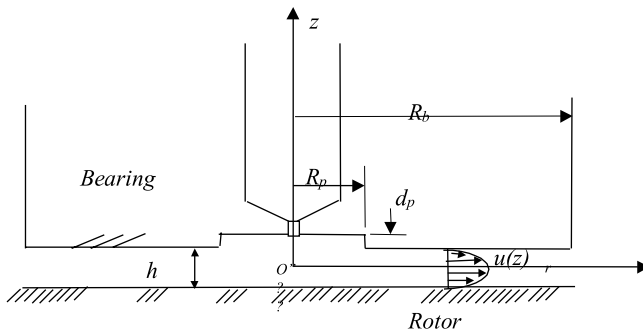


Fig. 3. Orifice compensated air bearing.

The time rate of change of the air mass is the difference between the inflow and the outflow, or

$$\frac{dm}{dt} = q_R - q_o, \quad (8)$$

where m is the mass of the air contained between the bearing surfaces; and q_R and q_o are the mass flow rate through the orifice restriction and the exhaust, respectively. The mass m is given by

$$m = 2\pi \left[\int_0^{R_p} (d_p + h)\rho r \, dr + \int_{R_p}^{R_b} h\rho r \, dr \right]$$

or

$$m = \frac{P_p}{RT} \pi R_p^2 (d_p + h) + \frac{2\pi}{RT} \int_{R_p}^{R_b} h\rho r \, dr. \quad (9)$$

Since the gap in the annulus is very small and the pressure variation in the z -direction is negligible, the flow between the surfaces is laminar. Thus, the flow–pressure relationship through the annulus, which is essentially laminar flow between two parallel surfaces, can be shown to be

$$p^2 = p_a^2 + \frac{12\mu q_o RT}{\pi h^3} \ln\left(\frac{R_b}{r}\right)$$

or we can express the flow rate as a function of pressure and the air gap as follows:

$$q_o = \frac{(p_p^2 - p_a^2)\pi h^3}{12\mu RT \ln(R_b/R_p)}. \quad (10)$$

The flow through an orifice has been modeled by several authors [9,26]. A particular form, known as Fliegner's approximation, has been chosen for this analysis due to its convenience for analytical and computational purposes.

$$q_R = 2 \left(\frac{\pi d_o^2}{4} \right) \left[\frac{\gamma}{RT} \left(\frac{2}{\gamma + 1} \right)^{(\gamma+1)/(\gamma-1)} (p_s p_p - p_p^2) \right]^{1/2}. \quad (11)$$

3.2. Energy conversion

The effect of the air gap on the rotor dynamics can be examined using the principle of energy conservation:

$$\vec{F}_b(t) \cdot \vec{v}(t) = \dot{E}_f, \quad (12)$$

where \dot{E}_f is the rate of the net fluid energy that is converted into mechanical energy; and F_b and \vec{v} are the corresponding converted mechanical force and velocity vectors, respectively. For multiple pairs of air bearings, the net fluid power is given by

$$\dot{E}_f = \sum_{i=1}^n \left[p_{si}q_{Ri} - p_{ai}q_{oi} - \frac{d}{dt} \left(\frac{1}{2} C_i p_{pi}^2 \right) \right], \tag{13}$$

where the air capacitance is defined as $C_i = dm_i/dp_{pi}$; and n is the number of air-bearing units.

Using Eq. (8), Eq. (13) can be rewritten as

$$\dot{E}_f = \sum_{i=1}^n \left[(p_{si} - p_{pi})q_{Ri} + (p_{pi} - p_{ai})q_{oi} - \frac{1}{2} p_{pi}^2 \dot{C}_i \right]. \tag{14}$$

The mechanical power can be written as

$$\vec{F}_b(t) \cdot \vec{v}(t) = \sum_{k=1}^3 F_{bk} \dot{X}_k, \tag{15}$$

where \dot{X}_k ($i = 1, 2, 3$) are the linear velocity components of the rotor or

$$dE_f = (\vec{F}_b \cdot \vec{v})dt = F_{bx}dx + F_{by}dy + F_{bz}dz. \tag{16}$$

Noting that the elements, dx , dy and dz , are independent of each other, the gradient of the total energy of the system gives the forces along the tangent lines; we have

$$\vec{F}_b = \nabla E_f, \tag{17}$$

where

$$\nabla \equiv \left(\frac{\partial}{\partial X_1} \right) \vec{E}_1 + \left(\frac{\partial}{\partial X_2} \right) \vec{E}_2 + \left(\frac{\partial}{\partial X_3} \right) \vec{E}_3$$

is the gradient of the system’s energy along the stator fixed coordinate axes.

In Eq. (14), the first and second terms account for fluid frictional dissipation in the orifice and in the annulus, respectively. The third term accounts for the fluid energy stored within the air gap, which depends on the volume change (capacitor) and the pressure in the air gap. To serve as an efficient air-bearing, the third term must dominate; otherwise the fluid energy will be dissipated as frictional heat. If the fluid frictional dissipation in the orifice and in the annulus are negligible; the system approaches the case of ideal energy transformation or

$$\vec{F}_{b,ideal} = \nabla E_f = -\frac{1}{2} \sum_{i=1}^n p_{pi}^2 \nabla C_i. \tag{18}$$

For a small air gap, the pressure in the annulus could be reasonably approximated by a linear relationship:

$$p \cong p_p - (p_p - p_a) \frac{r - R_p}{R_b - R_p}. \tag{19}$$

Substituting p from Eq. (19) into Eq. (9), we have

$$m \cong \frac{[h_i p_p A_{\text{eq}} + d_p p_p \pi R_p^2 + h_i p_a (\pi R_b^2 - A_{\text{eq}})]}{RT}, \quad (20)$$

where

$$A_{\text{eq}} = \pi R_{\text{eq}}^2 = \frac{\pi}{3} (R_b^2 + R_b R_p + R_p^2).$$

Using the definition of the air capacitance and Eq. (20), the following approximation can be derived:

$$C_i \cong \frac{[h_i A_{\text{eq}} + d_p \pi R_p^2]}{RT}, \quad (21)$$

$$\bar{F}_{\text{b,ideal}} \cong -\frac{A_{\text{eq}}}{2RT} \sum_{i=1}^n p_{pi}^2 \nabla h_i. \quad (22)$$

As shown in Eqs. (18) and (25), the air-bearing force is a quadratic function in p_{pi} . In addition, the force increases as the air gap (or the capacitance) decreases, which tends to stabilize about a steady-state operating point.

3.3. Perturbation model

In general, frictional dissipation cannot be neglected and the flow–pressure relationships, given by Eqs. (10) and (11), are highly non-linear. For the study of the dynamics due to a small deviation of the rotor displacement as shown in Fig. 2, we derive a perturbation model about an equilibrium operating condition (where the rotor is concentric with the stator).

Using the linear approximation of pressure along the annulus, the total force acting on the rotor is obtained by integrating the pressure over the bearing surfaces.

$$\tilde{f} = 2\pi \left[\int_0^{R_p} (\tilde{p}_{pi} - \tilde{p}_{pj}) r \, dr - \int_{R_p}^{R_b} (\tilde{p}_{pi} - \tilde{p}_{pj}) \frac{r - R_p}{R_b - R_p} r \, dr \right], \quad (23)$$

where the first integrand is at the pocket and the second is from the bearing annulus; the “ \sim ” over the variables denotes variation from equilibrium values.

$$\tilde{f} = \tilde{p}_p A_{\text{eq}}, \quad (24)$$

where $\tilde{p}_p = \tilde{p}_{pi} - \tilde{p}_{pj}$. In Eq. (24), the deviation of the pocket pressure p_p depends on the flow–pressure characteristics of the bearing. Since there is no contact between the surfaces, the frictional effect of air is negligible. The equation of rotor motion along the direction of the actuating force is thus

$$m_i \ddot{h}_i = A_{\text{eq}} \tilde{p}_p. \quad (25)$$

At equilibrium, since the gap h is equal to h_e (where the subscript ‘e’ denotes that the variables are evaluated at the steady state) and there is no change of air stored in

the bearing, the flow through the orifice is equal to that through the annulus, q_e . To the first degree of Taylor series approximation, the small deviation of the flow rate through the restrictor about the equilibrium can be written as

$$\tilde{q}_R = -a_1\tilde{p}_p + a_2\tilde{p}_s, \tag{26}$$

where $\tilde{p}_s = \tilde{p}_{si} - \tilde{p}_{sj}$; $\tilde{q}_R = \tilde{q}_{ri} - \tilde{q}_{Rj}$;

$$a_1 = \left(\frac{\partial(q_R)}{\partial p_p} \right) \Big|_{\substack{p_p=p_{pe} \\ q_R=q_e}} = \frac{q_e}{2p_s} \left(\frac{2 - (p_s/p_{pe})}{(p_s/p_{pe}) - 1} \right) \quad \text{and}$$

$$a_2 = \left(\frac{\partial q_R}{\partial p_s} \right) \Big|_{\substack{q_R=q_e \\ p_p=p_{pe}}} = \frac{q_e}{p_s - p_{pe}}.$$

The corresponding linear approximation of the flow rate through the annulus about the equilibrium condition can be derived from Eq. (10), which yields

$$\tilde{q}_o = a_3\tilde{p}_p + a_4\tilde{h}_i, \tag{27}$$

where

$$a_3 = \left(\frac{\partial(q_o)}{\partial p_p} \right) \Big|_{\substack{q_o=q_e \\ p_p=p_{pe}}} = \frac{2q_e p_{pe}}{(p_p^2 - p_a^2)} \quad \text{and} \quad a_4 = \left(\frac{\partial(q_o)}{\partial h_i} \right) \Big|_{h_i=h_e} = \frac{3q_e}{h_e},$$

where $\tilde{q}_o = \tilde{q}_{oi} - \tilde{q}_{oj}$; and note that $\tilde{h}_j = -\tilde{h}_i$. As shown in Eq. (8), the difference between the flow through the restriction and through the annulus is stored in the bearing, and its linear approximation is given as follows:

$$\frac{d\tilde{m}}{dt} = a_5\dot{\tilde{p}}_p + a_6\dot{\tilde{h}}_i, \tag{28}$$

where

$$a_5 = \left(\frac{\partial m}{\partial p_p} \right) \Big|_e = \frac{A_{eq} h_e + d_p \pi R_p^2}{RT}$$

and

$$a_6 = \left(\frac{\partial m}{\partial h_i} \right) \Big|_e = \frac{A_{eq}(p_{pe} - p_a) + \pi R_b^2 p_a}{RT}.$$

Hence,

$$a_5\dot{\tilde{p}}_p + a_6\dot{\tilde{h}}_i = (-a_1\tilde{p}_p + a_2\tilde{p}_s) - (a_3\tilde{p}_p + a_4\tilde{h}_i). \tag{29}$$

To explicitly obtain a dynamic equation in terms of h_i , we eliminate the pressure p_p by substituting it and its time derivative from Eq. (25) into Eq. (29). The resulting equation of the rotor motion is given by

$$\ddot{\tilde{h}}_i + \left(\frac{a_1 + a_3}{a_5} \right) \dot{\tilde{h}}_i + \left(\frac{A_{eq} a_6}{a_5 m_r} \right) \dot{\tilde{h}}_i + \left(\frac{A_{eq} a_4}{a_5 m_r} \right) \tilde{h}_i = \left(\frac{A_{eq} a_2}{a_5 m_r} \right) \tilde{p}_s. \tag{30}$$

Using Routh–Hurwitz stability criteria, the condition for an asymptotically stable system implies

$$\frac{(a_1 + a_3)a_6}{a_4a_5} > 1,$$

which yields

$$\frac{1}{3} \left[\frac{(3/2)p_s - p_{pe}}{p_s - p_{pe}} \right] > 1$$

or $p_{pe} > (3/4)p_s$. In addition, all the coefficients must be positive for stability, which implies that $p_{pe} < p_s$. Hence,

$$\frac{3}{4} < \frac{p_{pe}}{p_s} < 1. \tag{31}$$

3.4. Design tradeoff

Consider the case where the supply pressure is constant ($\tilde{p}_s = 0$). In other words, the air-bearing system is essentially a passive regulator. Note that the system is third-order and thus at least one of the characteristic roots is real which implies that Eq. (30) can be written in the following form:

$$(s + \sigma)(s^2 + 2\xi\omega_n s + \omega_n^2) = 0. \tag{32}$$

By expanding Eq. (32) and equating its coefficients to the corresponding terms in Eq. (30), the design parameters (σ , ξ and ω_n) can be related to the system parameters as follows:

$$\sigma + 2\xi\omega_n = \frac{c_2}{(1 + c_a(d_p/h_e))} \frac{q_e}{h_e}, \tag{33a}$$

$$\omega_n^2 + 2\xi\omega_n\sigma = \frac{c_1}{h_e(1 + c_a(d_p/h_e))}, \tag{33b}$$

$$\sigma\omega_n^2 = \frac{c_o}{(1 + c_a(d_p/h_e))} \frac{q_e}{h_e^2}, \tag{33c}$$

where

$$c_2 = \frac{RT}{A_{eq}} \left[\frac{2p_{pe} - p_s}{2p_{pe}(p_s - p_{pe})} + \frac{2p_{pe}}{p_{pe}^2 - p_a^2} \right], \tag{34a}$$

$$c_1 = \frac{A_{eq}(p_{pe} - p_a) + \pi R_b^2 p_a}{m_r}, \tag{34b}$$

$$c_o = \frac{3RT}{m_r}, \tag{34c}$$

$$c_a = \frac{\pi R_p^2}{A_{eq}}. \tag{34d}$$

Note that A_{eq} is generally constrained by the spherical actuator geometry. Thus, Eqs. (33a)–(33c) represent the design trade-off among the three design variables, q_e , h_e , and d_p for a specified dynamic response, which can be expressed as

$$q_e = \frac{1+n}{1+4n\xi^2} \frac{c_1}{c_2\omega_n}, \quad (35)$$

$$h_e = \frac{1+n}{n} \frac{c_o}{c_2\omega_n^2}, \quad (36)$$

$$d_p = \frac{c_o}{c_a c_2 \omega_n^2} \left(\frac{c_1 c_2}{c_o} \frac{1}{1+4n\xi^2} - \frac{n+1}{n} \right), \quad (37)$$

where $n = (2\xi\omega_n)/\sigma$. The effect of the third pole could be reduced if σ is large compared to $\xi\omega_n$ (or $n \gg 1$). However, for a practical air-bearing system, the pocket depth must be real, finite and positive; it thus imposes a constraint on the choice of ω_n , σ , and ξ .

4. Bearing design for spherical actuator

The distribution of bearings on the spherical rotor determines the support forces generated. To maintain the rotor in equilibrium at the stator center, the air bearings are designed to direct their forces at the vertices of polyhedrons towards the stator center. Thus, once the bearing locations are specified, the directions of the forces are considered known.

Theoretically, the minimum number of simple point bearings required to achieve bi-directional position control of the spherical rotor in a three-dimensional space is four. To illustrate the minimum force requirement, consider three forces that are directed radially toward the origin O of a fixed reference frame. The three points $P_1(x, y, z), P_2(x, y, z), P_3(x, y, z) \in E^3$ are on a plane defined by $\Pi(P_1P_2, P_1P_3)$. Since the points at which the forces act are coplanar, any disturbance in the orthogonal direction to this plane consisting of the line $(P_1P_2 \times P_1P_3)$ will cause the rotor to lose its equilibrium, since the actuating forces are only acting in the direction toward the rotor center. Thus, three point bearings are not adequate to control all three orthogonal translations of the rotor. A fourth line of action must be applied against the plane containing the three points. A possible arrangement of the minimum number of point bearings on a spherical surface is to locate them at the vertices of a regular tetrahedron on which the sphere is inscribed. A disadvantage of this configuration is that the four point bearings cannot be arranged in pairs for a push-pull (regulation) control strategy. The arrangement of bearings is not necessarily attractive, since four independent actuators are required.

Table 2
Icosahedron vertices

| Vertices | <i>X</i> | <i>Y</i> | <i>Z</i> |
|------------------------|----------|----------|----------|
| <i>c</i> ₁ | 0.89442 | 0 | 0.44721 |
| <i>c</i> ₂ | 0.27639 | 0.85065 | 0.44721 |
| <i>c</i> ₃ | -0.72361 | 0.52573 | 0.44721 |
| <i>c</i> ₄ | -0.72361 | -0.52573 | 0.44721 |
| <i>c</i> ₅ | 0.27639 | -0.85065 | 0.44721 |
| <i>c</i> ₆ | -0.89443 | 0 | -0.44721 |
| <i>c</i> ₇ | -0.27639 | -0.85065 | -0.44721 |
| <i>c</i> ₈ | 0.72360 | -0.52573 | -0.44721 |
| <i>c</i> ₉ | 0.72360 | 0.52573 | -0.44721 |
| <i>c</i> ₁₀ | -0.27639 | 0.85065 | -0.44721 |

4.1. Design configuration

An alternative arrangement is to locate the bearings at the vertices of polyhedrons, in an arrangement similar to that of the stator pole arrangement for a spherical motor [8]. For polyhedrons such as hexahedrons, octahedrons, icosahedrons, and dodecahedrons, bearings can be arranged in pairs with their supporting forces directed radially toward the center of the sphere. Other advantages include the following: (1) It could be integrated as a part of the stator pole, so that pressurized air passes through the center of the electromagnetic pole enabling it also to serve as a bearing. (2) The air-jet will provide a cooling effect on the electromagnetic pole coil windings. An example layout is given in Table 2, where 10 of the 12 vertices following the pattern of a unit icosahedron are listed.

The 3D rotor dynamics is of the form:

$$[m_r]\ddot{\mathbf{X}} = \mathbf{F}_m + \mathbf{F}_b, \quad (38)$$

where \mathbf{F}_m and \mathbf{F}_b are the resultant electromagnetic and air-bearing force vectors, respectively. In this air-bearing system control, the magnetic force \mathbf{F}_m is treated as an external disturbance. As shown in Table 2, five pairs of bearings can be located diametrically on c_i/c_{i+5} ($i = 1, 2, \dots, 5$), which pass through the center of the outer sphere. Thus, the air-bearing force \mathbf{F}_b is a sum of the component force vectors contributed by these five independent pairs of bearings.

4.2. Design of single air-bearing pair

Figs. 4(a) and (b) show the pocket depth plotted as a function of natural frequency and damping ratio, respectively. As h_c and d_p are inversely proportional to ω_n^2 , we chose $\omega_n = 240$ Hz (or 1508 rad/s), $\sigma = 2\xi\omega_n$ (or $n = 1$) and $\xi = 0.5$ to provide a reasonable physical size for the pocket depth and the air gap and to provide an acceptable dynamic response. Given the rotor mass of an existing spherical motor and the available surface area for the bearings, the corresponding calculated pa-

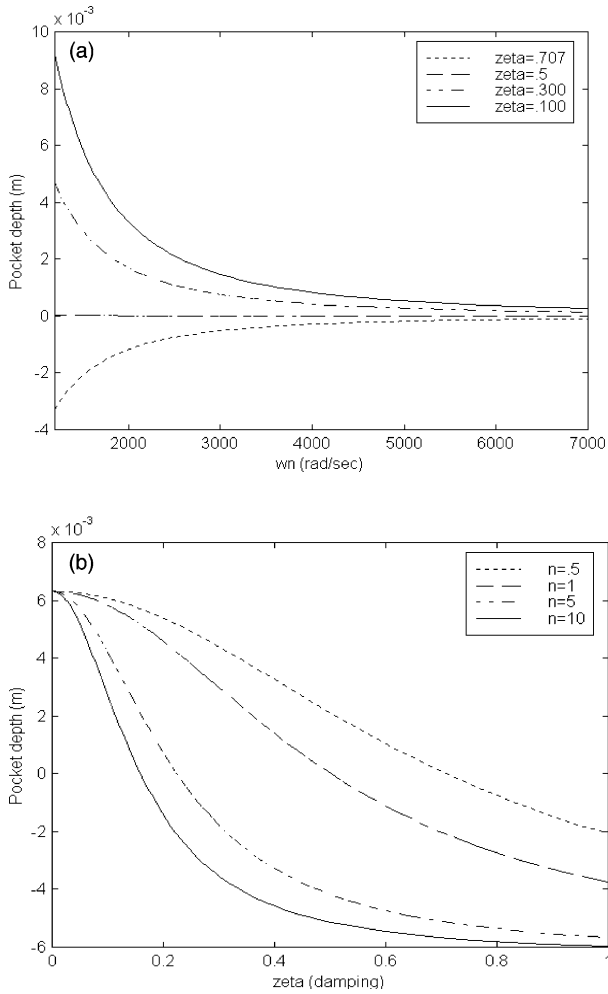


Fig. 4. Effect of ω_n and ζ on the choice of pocket depth. (a) Pocket depth vs natural frequency ($n = 1$). (b) Pocket depth vs damping ratio ($\omega_n = 240$ Hz).

parameters are $q_e = 1.281e-5$ kg/s, $h_e = 0.069$ mm and $d_p = 0.019$ mm. Table 3 summarizes the parameters determined from the trade-offs.

Fig. 5 shows the rotor displacement in the direction of actuating force for an initial displacement of $5.8 \mu\text{m}$, respectively. As shown in Fig. 5, the rotor returns to its equilibrium in less than 5 ms.

4.3. Simulation results of the 3D rotor dynamics

The spherical air-bearing system is simulated using MATLAB for the three degrees-of-freedom rotor translations. In order to examine the effect of trajectory-dependent magnetic forces during operation, we simulate the 3D rotor dynamics under the

Table 3

Parameters used in simulation

| Parameters | Values used |
|------------------------------|-----------------------|
| Mass, m_r | 0.2 kg |
| Outer radius, R_b | 12.7 mm |
| R_b/R_p | 16 |
| Supply pressure, p_s | 420 kN/m ² |
| Pressure ratio, p_{pc}/p_s | 0.92 |
| Pocket depth, d_p | 19.3 μm |
| Orifice diameter | 0.225 mm |
| Nominal, h | 69 μm |

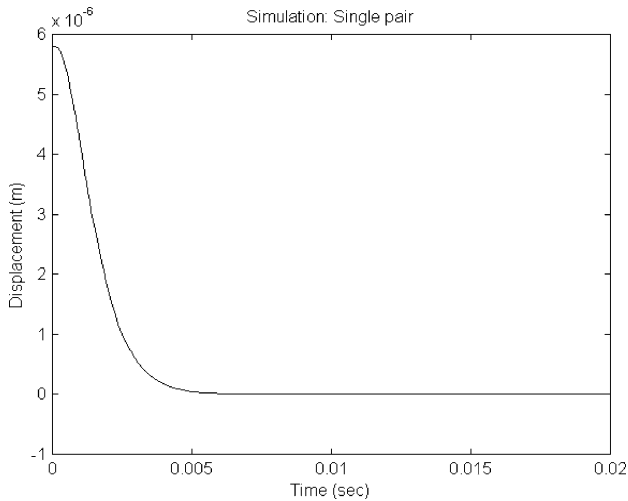


Fig. 5. Rotor displacement (1-d.o.f.).

influence of an external force function as shown in Fig. 6. The simulation results are plotted in Fig. 7. The results indicate that the external disturbance is adequately compensated by the air-bearing system, since the force has little impact on the air bearing dynamics.

Since the models have been derived using perturbation analysis, it is of interest to examine the range of this approximation. Fig. 8 shows the comparison between the linearized and the non-linear models about the operating condition. Within $\pm 25\%$ of the equilibrium value, the difference between the actual and the approximate perturbation flow rates is only 0.778%. The deviation increases as the operating point is moved to a reduced pocket pressure (i.e. reduced pressure ratio). This implies that the operating pocket pressure fluctuates between $3.7\text{e-}5$ and $3.9\text{e-}5$ N/m² for this design. The actual downstream pressure at the edge of the pocket is much less (see Table 3) due to expansion and corner losses.

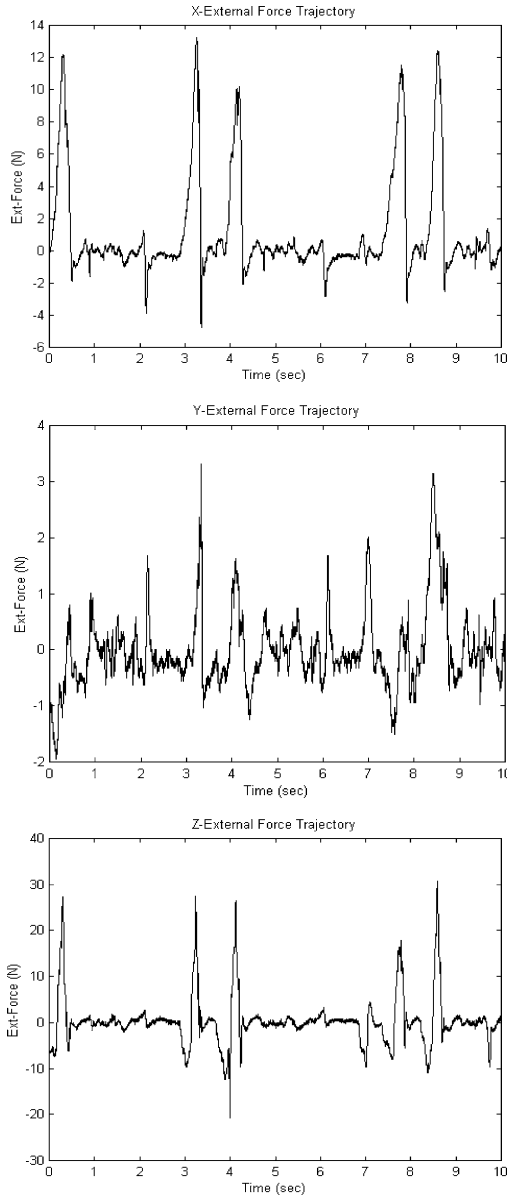


Fig. 6. External force trajectory.

The design methodology has led to an improved dynamic performance by reducing contact friction. The torque improvement by using air bearing in place of transfer bearings on the VR spherical is the total torque loss due to the transfer bearings. It has been estimated that the maximum radial electromagnetic force is 65

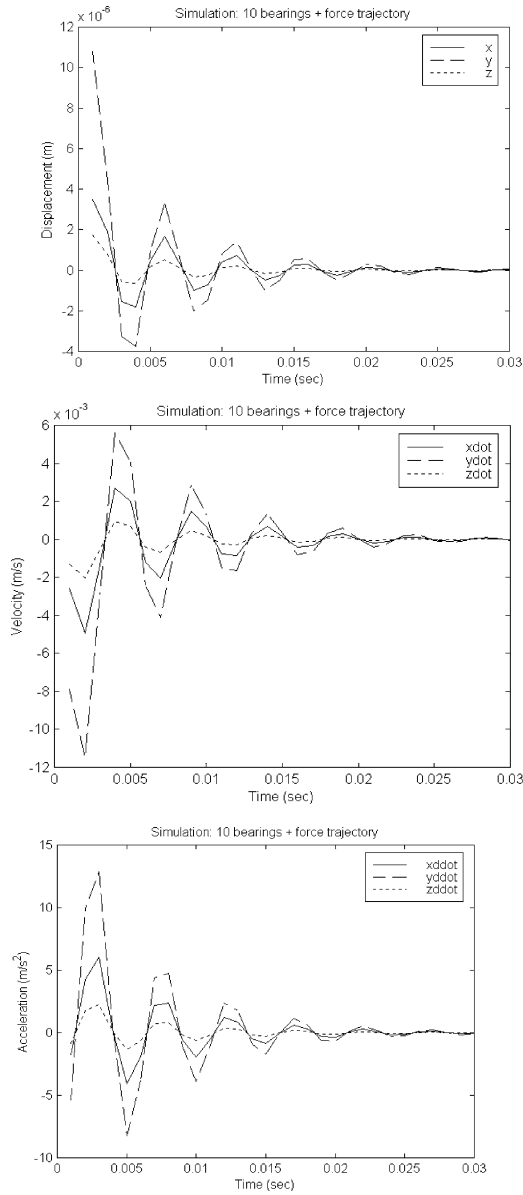


Fig. 7. Simulated rotor motion.

N for a particular rotor orientation [27]. For a uniform operating radial force of 32.5 N over eleven transfer bearings and a contact friction coefficient of 0.05 between the rotor and the plastic transfer bearings, the potential torque gain is 27.17% of the rated torque. In addition, the air-bearing design has also reduced potential sources of uncertainty to the control design of the VR spherical motor.

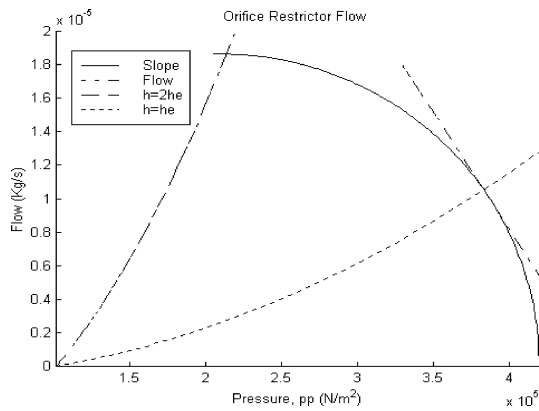


Fig. 8. Equilibrium operating point.

5. Conclusions

We have presented the method for design of a practical air-bearing system for a VR spherical motor. Specifically, this paper has addressed the following fundamental issues of the bearing system design:

1. The method of generating the necessary rotor support forces with externally pressurized air and the strategic arrangement of point bearings is discussed. The design uses strategic placement of bearings at the vertices of polyhedrons and external pressurized air to regulate the rotor translations.
2. The forward and inverse kinematics between the rotor displacement and the individual air gaps at positions round the stator are developed in closed-forms, which are essential for design, dynamic simulation and control purposes.
3. Along with the pressure–flow relationship as a function of the rotor position, the paper presented a detailed dynamic model of the air bearing. Trade-off between the design parameters and the dynamic performance of the air-bearing regulator system have been discussed with a design example.

The studies have led to the design of a potentially useful air-bearing system capable of eliminating frictions in ball-joint-like actuators. The dynamic performance of the air-bearing system has been evaluated analytically by simulation. It is expected that this research will be a basis for designing and evaluating an improved VR spherical motor with enhanced torque capability by eliminating mechanical friction.

References

- [1] Hamcock BJ. Fundamentals of fluid film lubrication. New York: McGraw-Hill; 1994.
- [2] Renshaw AA. The stability of flexible spinning disks supported by incompressible hydrodynamic lubrication. In: International Symposium on Information Storage and Processing Systems, ASME/ISPS-Vol. 2, Atlanta, GA, 1996 Nov 17–22. p. 175–9.

- [3] Trumpler PR. Design of film bearing. New York: Macmillan; 1966.
- [4] Fearing RS. Micro structures and micro actuators for implementing sub-millimeter robots, excerpts from precision, sensors, actuators and system. Netherlands: Kluwer Academic Publishers; 1990. p. 39–72.
- [5] Pina da Silva F. Squeeze film air bearing with flexible support. Ph.D. Thesis. England: Imperial College; 1980.
- [6] Pina da Silva F, Almas EM. Recent developments in the theory of squeeze film bearings. *Tribol Int* 1986;19(2):79–86.
- [7] Crank J, Nicholson P. A practical method for numerical evaluation of solutions for partial differential equation of the heat conduction type. *Proc Cambridge Philos Soc* 1947;42:50–67.
- [8] Blech JJ. On isothermal squeeze films. *ASME J Lubrication Technol* 1983;105:615–20.
- [9] Sherman FS. Viscous flow. New York: McGraw-Hill; 1990.
- [10] Zorge RA. Measurements on a miniature spherical air bearing using its electrical gap capacitance. *J Measure* 1993;11:159–72.
- [11] Licht L, Fuller DD, Sternlicht B. Self-excited vibrations of an air-lubricated thrust bearing. *Trans ASME* 1958;80:411–4.
- [12] Licht L, Elrod H. A study of the stability of externally pressurized gas bearings. *ASME J Appl Mech* 1960;82:250–8.
- [13] Wilcock DF. MTI gas bearing design manual. Latham, NY: Mechanical Technology; 1972.
- [14] Ono K. Circumferential grooved hydrostatic gas thrust bearing 1st report, characteristics in low pressure region. *Trans JSME* 1988;51(468):2009–16.
- [15] Mori H, Mori A, Kaneko R, Yoshida K. Stability element for external pressurized gas bearing 2nd report, stabilizing element inserted into the gas supply line. *Trans JSME* 1966;32(244):1883–2064.
- [16] Ohsumi T, Ikeuchi K, Mori H, Haruyama HJ, Matsumoto Y. Characteristics of a hydrostatic bearing with a controlled compensating element. *Wear* 1991;105:177–94.
- [17] Sato Y, Murata K, Harada M. Dynamic characteristics of hydrostatic thrust air bearing with actively controlled restrictors. *Trans ASME Tribol Conf* 1988;110(1):156–61.
- [18] Hammer R, Hollis RL, An CH, Hendricks F. Design and control of an air bearing supported three degree of freedom fine positioner. In: *Proceedings of the IEEE International Conference on Robotics and Automation*, Nice, France, 1992. p. 677–84.
- [19] Okada Y, Saitoh T, Shinoda Y. Vibration control of flexible rotor supported by inclination control magnetic bearings. *AIM'99 Proceedings*, Atlanta, GA. p. 788–93.
- [20] Ueno S, Okada Y. Vector control of an induction-type axial gap combined motor-bearing. *AIM'99 Proceedings*, Atlanta, GA. p. 793–9.
- [21] Setiawan JD, Mukherjee R. Adaptive compensation of sensor runout and mass unbalance in magnetic bearing systems. *AIM'99 Proceedings*, Atlanta, GA. p. 800–5.
- [22] Lee K-M, Roth R, Zhou Z. Dynamic modeling and control of a ball-joint-like variable reluctance spherical motor. *ASME J Dyn Syst, Measure Control* 1996;118(1):29–40.
- [23] Zhou Z, Lee K-M. Characterization of a three degrees-of-freedom variable-reluctance spherical motor. *J Syst Eng (Special issue on Motion Control)* 1994;4:60–9.
- [24] Lee KM, Meyouhas G, Blenis R. A machine-vision-based wrist sensor for direct measurement of three degrees-of-freedom orientation. *Mechatronics* 1993;3(5):571–87 (also presented in *Proceedings of the 12th World Congress of International Federation of Automaticvol*, vol. VIII, Sydney, Australia, 1993 July 18–23. p. 493–9).
- [25] Zhou Z, Lee K.-M, A high precision torque control of a self magnetically-levitated six-d.o.f. VR spherical motor. In: *1994 ASME IMECE*, Chicago, IL, vol. 55–1, 1994 Nov 6–11. DSC. p. 775–80.
- [26] Slocum AH. Precision machine design. Englewoodcliffs, NJ: Prentice-Hall; 1992.
- [27] Roth, R. B., An experimental investigation and optimization of a variable reluctance spherical motor. Ph.D. Thesis, Mechanical Engineering, Georgia Tech., 1992.